# Analysis of light propagation characteristic in the aero-optic flow field of cone-headed vehicle with side window*

**XU Liang[1]**, ZHOU Liye[1], WANG Luyang[1], ZHAO Shiwei[1], and WANG Tao[2,3]**

*1. Tianjin Key Laboratory of Complex Control Theory and Application, School of Electrical Engineering and Automation, Tianjin University of Technology, Tianjin 300384, China*

*2. School of Intelligent Engineering, Sun Yat-sen University, Guangzhou 510275, China*

*3. Southern Marine Science and Engineering Guangdong Laboratory (Zhuhai), Zhuhai 519000, China*

(Received 10 May 2023; Revised 4 July 2023)



Aero-optic imaging deviation research is carried out for infrared-guided vehicle with cone-head side window, with a focus on the propagation characteristics of light in an aero-optic flow field. When the light entering the aero-optic flow field from the free-stream should be close to the normal, numerous data indicate that the light is refracted away from the normal. This paper divides the aero-optic flow field into two parts and uses the gas density distribution in the aero-optic flow field to propose the hypothesis that there are two modes of refraction when light propagates through the flow field. The results show that light propagates from the optically denser medium to the optically thinner medium after passing through the shock wave and eventually leads to refraction away from the normal when the light enters the aero-optic flow field.

**Document code:** A **Article ID:** 1673-1905(2024)01-0058-7

**DOI** https://doi.org/10.1007/s11801-024-3083-8

Aero-optics is an interdisciplinary discipline involving optics, fluid mechanics, optoelectronics and other multidisciplinary fields, and has a wide range of applications in both military and civil applications[1,2]. The air around the vehicle is ionized to form a plasma sheath that is difficult to be penetrated by electromagnetic waves[3]. To facilitate communication, an optical window is added to the head of a high-speed vehicle[4]. The cavity structure formed at the optical window results in a more complex flow field and more pronounced aero-optic effects near the head of the vehicle[5,6]. For beam transmitted in aero-optical flow field, the backward ray tracing method is used for tracking, reducing the redundant calculations in conventional forward tracing method[7]. WANG et al[8] studied the effect of altitude (*Alt*) on the degradation of the aerodynamic optical imaging quality of the hemispherical optical dome: the influence of aerodynamic optical effects diminished with increasing *Alt*. GUO et al[9] investigated the aero-optical effects of an optical seeker with a supersonic jet for hypersonic vehicles in near space. The results show that aero-optical effects are quite weak when the *Alt* is greater than 30 km, and the imaging displacement is related to the incident angle of a beam. YAO et al[10] showed the effect of the target line of sight (LOS) angle on the aerial optics imaging deviation in a wide range of 5°—85°. As the LOS angle increases, the aero-optical imaging deviation gradually decreases. WANG et al[11] noted that as the angle of attack increases from 0°—15°, the refractive index and aero-optical imaging deviation increase. XU et al[12,13] argued that physical quantities such as flight altitude and Mach number don't directly affect the imaging deviation; these factors affect the gas density around the vehicle, which leads to the change in the propagation path of the ray, which in turn leads to the imaging deviation. According to the principle of optical refraction, light entering optically denser medium from optically thinner medium should behave in the direction of refraction close to the normal[14]. Based on this finding, this paper focuses on the propagation characteristics of light in aero-optic flow field. By calculating the imaging deviation and the deflection angle data for different operating conditions and combining them with the flow field density variation, the refraction path of light in the flow field is further decomposed and the reason why the refraction of light in the aero-optic flow field behaves away from the normal is explained.

The overall simulation process can be broadly divided into three parts: pre-processing, solution calculation and post-processing[15]. The pre-processing process mainly

* This work has been supported by the National Natural Science Foundation of China (Nos.61975151 and 61308120).

** E-mail: liangx999@163.com

uses SCDM to build model, which is shown in Fig.1.

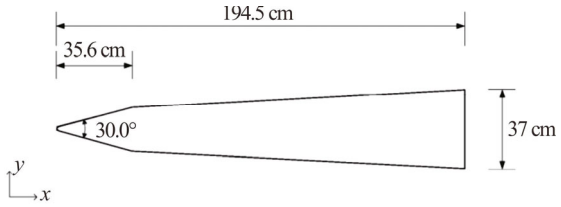


**Fig.1 Model of the vehicle**

Afterwards, the head region and the external flow field part of the model are meshed in integrated computer engineering and manufacturing (ICEM). The mesh size as small as possible to ensure a reasonable number of meshes, which helps to improve the accuracy of the subsequent solution[16]. The result of the mesh generated is shown in Fig.2, mesh quality is above 0.8, and the total grid cells are 167 284.

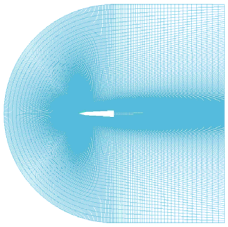

**Fig.2 Meshing of the outflow field**

The solution is calculated by importing the mesh file processed by ICEM into Fluent and setting the solver, material and boundary conditions. The main flow is shown in Fig.3.

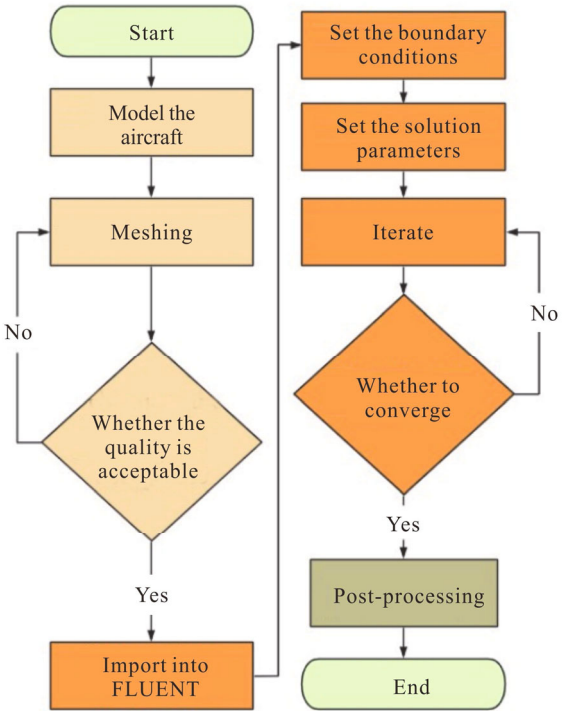


**Fig.3 Simulation flow chart**

HAO et al[17] found that the deviation produced at the flat optical window would be smaller, so the mathematical models of aero-optical transmission constructed in the paper are for the flat optical window. The imaging deviation caused by aero-optic effect is mainly influenced by the mean flow field, so the realizable $k-\varepsilon$ two-equation model in Reynolds averaging method is chosen in this paper to solve the density data, which can more accurately simulate the diffusion velocity of planar and circular jets, while the calculation results are more in line with the rotating flow calculation, boundary layer calculation with directional pressure gradient and separation flow calculation when the realistic conditions[18,19].

Although the two-equation model is not yet a complete description of complex aero-optical flow fields, and higher-order turbulence models that consider the turning zone or solve more partial differential equations can theoretically yield more accurate solutions, successful comparisons of computational cases and experimental results from numerous research units within the discipline show that invoking $k-\varepsilon$ or $k-\omega$ models integrated in packages such as Fluent, FASTRAN, etc, and considering high-temperature gas mixtures, the additional energy equation in the solution equation, and the mass conservation equation of the chemical components are fully feasible in the ray-tracing engineering calculations for the imaging deviation involved in this study[11].

The transport equations for $k$ and $\varepsilon$ in the realizable $k-\varepsilon$ two-equation model are as follows

$$\frac{\partial(\rho k)}{\partial t}+\frac{\partial(\rho k u_i)}{\partial x_i}=\frac{\partial}{\partial x_j}\left[\left(\mu+\frac{\mu_t}{\sigma_k}\right)\frac{\partial k}{\partial x_j}\right]+G_k-\rho\varepsilon, \tag{1}$$

$$\frac{\partial(\rho\varepsilon)}{\partial t}+\frac{\partial(\rho\varepsilon u_i)}{\partial x_i}=\frac{\partial}{\partial x_j}\left[\left(\mu+\frac{\mu_t}{\sigma_\varepsilon}\right)\frac{\partial \varepsilon}{\partial x_j}\right]+\rho C_1 S\varepsilon-\rho C_2\frac{\varepsilon^2}{k+\sqrt{\nu\varepsilon}}. \tag{2}$$

Once the flow field density data has been obtained, the density needs to be converted to refractive index to calculate imaging deviation. In optical calculations, the Gladstone-Dale (G-D) relationship is a quantitative equation that describes the relationship between refractive index and density. The G-D coefficient for standard air is a weak function of wavelength[20], and when the density $\rho$ is expressed as kg/m$^3$ and the wavelength $\lambda$ as μm, the G-D coefficient can be approximated as

$$K_{GD}=2.23\times10^{-4}\left(1+\frac{7.52\times10^{-3}}{\lambda^2}\right). \tag{3}$$

When a vehicle with an optical imaging detection system is travelling at high speed through the free-stream, the gas compression between the optical hood and the incoming flow is very intense, creating a complex non-uniform

flow field around it. Taking Fig.4 as an example, the light is deflected as it enters the non-uniform flow field due to aero-optic effect. At this point there is a certain deviation between the position where the light arrives at the optical window and where it arrives after the free-stream without aero-optic effect, which is known as the aero-optic imaging deviation[21].

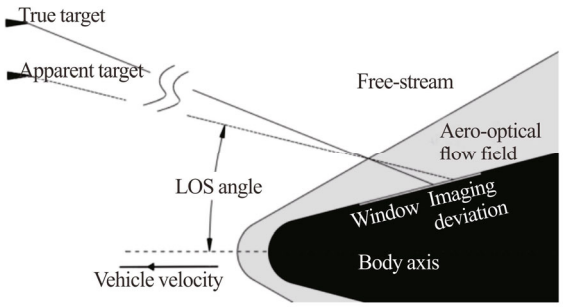


**Fig.4 Schematic diagram of the aero-optic imaging deviation**

The main factors that affect the aero-optic imaging deviation include altitude, Mach number, angle of attack and LOS angle. The LOS angle is the angle between the angle of incidence and the axis of the projectile[22]. As the relative position and attitude between the target and the vehicle changes, the LOS angle changes, causing the deflection angle of the light to be altered, which ultimately affects the imaging deviation. Computational fluid dynamics (CFD) computations were performed on the conical vehicle model to obtain a large number of imaging deviation for the vehicle at LOS angle ranging from 65° to 85°. Flight conditions are shown in Tab.1.

**Tab.1 Flight condition**

| Flight variable | Example 1 | Example 2 |
|---|---|---|
| Altitude | 40 | 50 |
| Mach number | 5 | 5 |
| Angle of attack | 0 | 0 |

The imaging deviation slope is used to reflect the sensitivity of the imaging deviation as the LOS angle changes[23], and is calculated by the finite difference method for the data in the example. With $d$ as the imaging deviation, $\Delta x$ as the step size of the correlation variable and $\nabla d$ as the slope of the imaging deviation of the correlation variable, the central difference format is

$$\nabla d = \frac{d_{i+1} - d_{i-1}}{2\Delta x}. \tag{4}$$

The left boundary of the sequence uses the first-order forward differential format as

$$\nabla d = \frac{d_{i+1} - d_i}{\Delta x}. \tag{5}$$

The right boundary of the sequence uses the first-order backward differential format as

$$\nabla d = \frac{d_i - d_{i-1}}{\Delta x}. \tag{6}$$

In this paper, the tracing step is set to 0.08 mm. The calculation results of Example 1 and Example 2 are shown in Fig.5 and Fig.6, respectively.

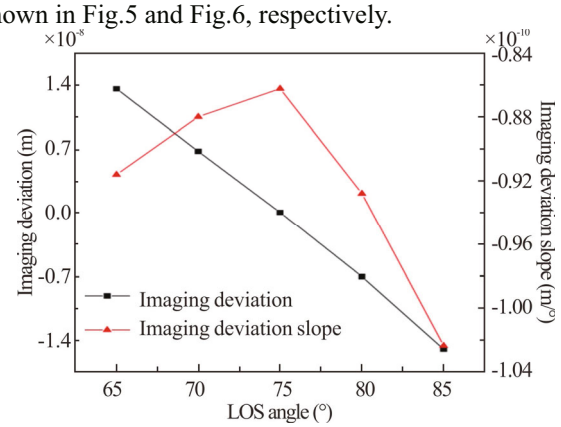


**Fig.5 Imaging deviation and slope of imaging deviation for Example 1**

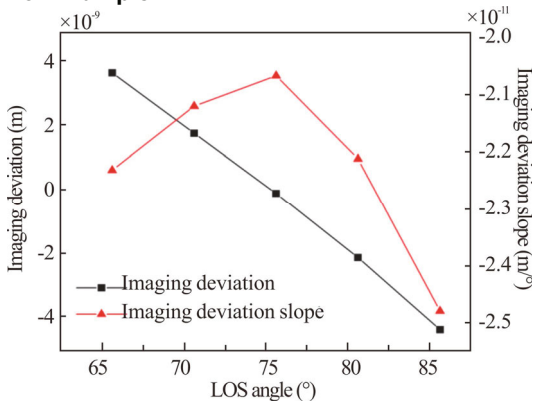


**Fig.6 Imaging deviation and slope of imaging deviation for Example 2**

According to Fig.5 and Fig.6, it can be seen that the trend of the curves in both figures is about the same for different flight conditions. The positive and negative of the imaging deviation in the figure only indicate the direction and don't represent the numerical value, the positive value represents the imaging deviation to the right at the optical window. According to the curves in the graphs, the imaging deviation and the slope of the imaging deviation decrease first and then increase in the range of 65°—85°, and the direction of the imaging deviation at the optical window is reversed.

The flow field boundary curve within the field of view of the optical window of the head of the high-speed vehicle is approximately straight. At high Mach number conditions at high altitude, the deformation of the aero-optical flow field is small. If the operating conditions are changed at this time, the LOS angle of the light incident vertically into the flow field will change slightly. However, because the LOS angle growth interval is 5° when the operating conditions are selected in this paper, the data are plotted to show that the imaging deviation is very close to zero at the LOS angle of 75°.

The light will be refracted after entering the aero-optic flow field boundary. The deflection angle is obtained by

subtracting the angle of refraction from the angle of incident. During the ray tracing process, each step generates the corresponding deflection angle, and the overall deflection angle can be derived by accumulating the step-by-step deflection angles. The deflection angle of light incident from the aero-optic flow field boundary to the optical window at the LOS angle of 60°—80° is plotted, the deflection angle is shown as negative in the clockwise direction and positive in the counterclockwise direction. The results of the deflection angle for Example 1 and Example 2 are shown in Fig.7.

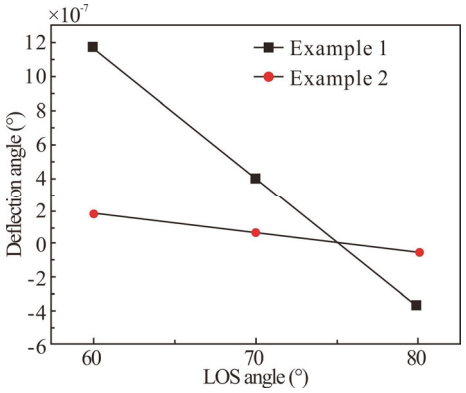


**Fig.7 Results for deflection angle**

Fig.7 shows that the deflection angle decreases and then increases as the LOS angle increases to the range of 60°—80°, with the direction reversed. It is similar to the physical law above in which the direction of the imaging deviation is reversed when the LOS angle is increased to the range of 60°—80°. It means that the light entering the aero-optic flow field is actually continuously refracted overall in the direction of the imaging deviation at the optical window.

With the flight conditions held constant and the incident light entered the aero-optic flow field from constant coordinates, changing only the direction of incidence can be seen as keeping the distance $D$ between the point of incidence of the light and the optical window constant. As shown in Fig.8, with the constant distance $D$, the magnitude of the imaging deviation ($L$) is proportional to the deflection angle ($\omega$) and the direction changes with the direction of the deflection angle.

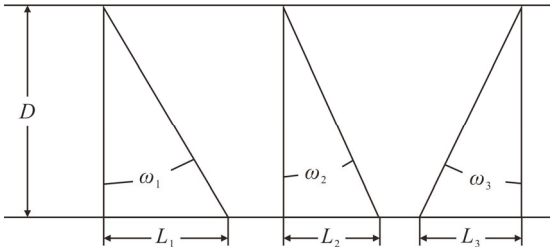


**Fig.8 Relationship between imaging deviation and deflection angle**

The analysis of imaging deviation and deflection angle in the previous section revealed that whatever the direction of the imaging deviation, it is reflected in the light transmission process as light is refracted away from the normal. The ray tracing diagram is shown in Fig.9.

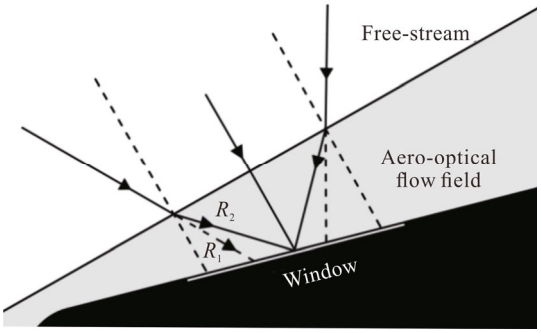


**Fig.9 Diagram of ray tracing**

In Fig.9, $R_1$ represents that if the flow field outside the vehicle is a uniform free-stream, the light will travel along the straight line to the optical window without deflection. However, during flight there is a large non-uniform aero-optic flow field surrounding the vehicle, and light will be refracted as it enters the aero-optic flow field from the free-stream. This means that the light in the diagram, which should travel along $R_1$ to the optical window, will deflect as it enters the aero-optic flow field and eventually follow $R_2$ to the optical window.

It is notable that the aero-optic flow field is essentially a compressed gas flow field, which is much denser than the free-stream. According to the theorem of refraction of geometrical optics, when light propagates from the optically thinner medium to the optically denser medium, the light will be refracted closer to the normal and the deflected light should be to the left of $R_1$. However, the large amount of data obtained from the calculation proves that the refraction law in Fig.9 is correct, which indicates that the light must additionally have been refracted from the optically denser medium to the optically thinner medium when propagating in the aero-optic flow field, which eventually causes the change of the overall refraction direction.

During the high-speed flight of the vehicle, the external gas is compressed by the sudden leap of the vehicle, producing a compressed surface with a certain intensity, called the shock wave[24]. This paper further divides the aero-optic flow field and names the aero-optic flow field boundary as $A$, the dividing line between the shock wave and the internal gas flow field as $B$, and the optical window as $C$. The density distribution on the light propagation path in the aero-optic flow field is plotted as the waterfall diagram at 65°—85° LOS angle, and the results of Example 1 and Example 2 are shown in Fig.10 and Fig.11, respectively. The $\gamma$ is normalization distance from a point to the window on the propagation path of the light.

Due to the backward ray tracing method used in the optical calculation, the ray travel from the optical window to the free-stream[25]. The figure shows that the

thickness of the shock wave between $A$ and $B$ is very thin compared to the aero-optic flow field of the vehicle, but there is a large leap in the density of the gas as it passes through the shock wave. This article infers that refraction of light from optically denser medium to optically thinner medium occurs after travelling through the shock wave due to the decrease in gas density. The deflection angle from $A$ to $B$ is denoted as $\delta$ and the deflection angle between $B$ and $C$ is denoted as $\zeta$, where the deflection angle is shown as negative in the clockwise direction and positive in the counterclockwise direction, and the graphs are made at 60°—85° LOS angle. The results of Example 1 and Example 2 are shown in Fig.12 and Fig.13.

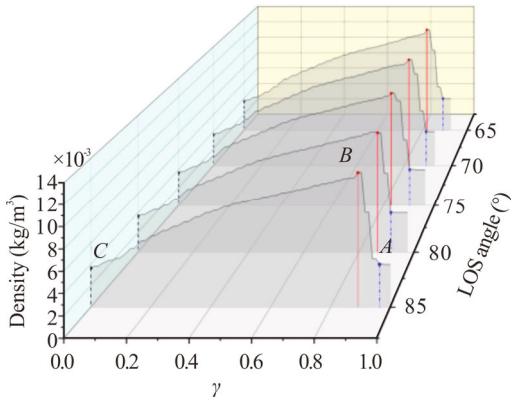


**Fig.10 Density distribution along the path of light propagation for Example 1**

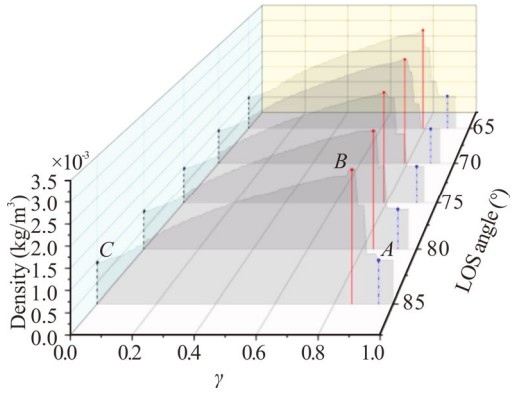


**Fig.11 Density distribution along the path of light propagation for Example 2**

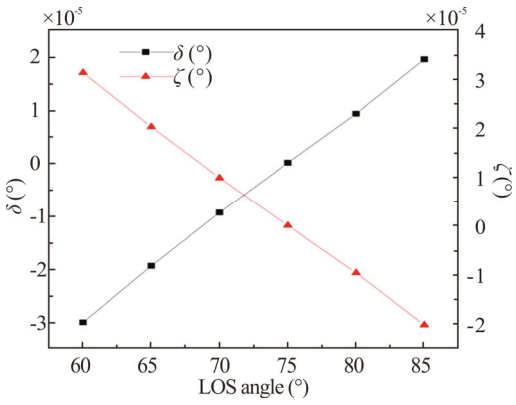


**Fig.12 Two deflection angles for Example 1**

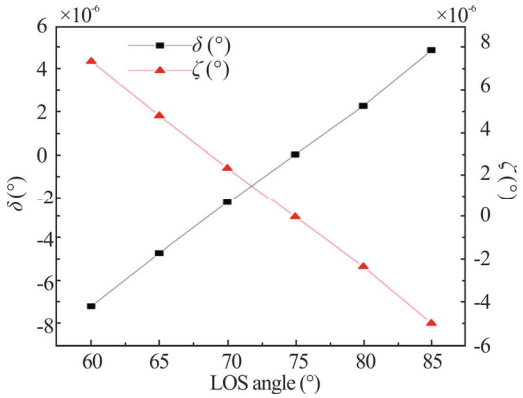


**Fig.13 Two deflection angles for Example 2**

The graph clearly shows that as the LOS angle increases, the values of $\delta$ and $\zeta$ both decrease and then increase, with a minimum value in the range of 70°—80°, which coincides with the physical law of deflection angle obtained above. It is also evident that $\delta$ and $\zeta$ always deflect in opposite direction at the same LOS angle, which proves that there are two types of refraction when light propagates in the flow field, close to the normal and far from it. Combined with the above analysis of the density distribution and the deflection angle in the flow field, the propagation path of light in the aero-optic flow field is given in Fig.14.

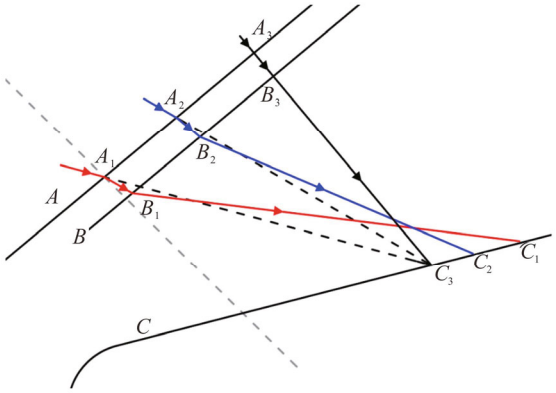


**Fig.14 Refraction path of light in the flow field**

Due to the large leap in density of the shock wave relative to the density of the free-stream, the light is deflected close to the normal between $A$ and $B$, and the deflection angle is relatively large. However, after the light passes through the shock wave, the density slowly decreases from $B$ to $C$. The light is refracted from optically denser medium to optically thinner medium. The light deflection is divided into two parts, $AB$ and $BC$. The $AB$ section has a large variation in density and a larger deflection angle, but $A_1B_1 \approx A_2B_2 \approx A_3B_3$ is smaller because the shock wave is thinner. Compared to the $AB$ section, the light has a very obvious increase in propagation distance in the $BC$ section. If the $BC$ section is cut by differentiation, the light can be seen as constantly refracting from optically denser medium to optically

thinner medium in the *BC* section, which is shown by the light continuously propagating away from the normal, resulting in the value of the deflection angle $\zeta$ between *BC* that is greater than the value of the deflection angle $\delta$ between *AB*.

In this article, with a focus on the propagation characteristic of light in the aero-optic flow field, through extensive simulation experiments and analysis of the results, the following conclusions were obtained.

The imaging deviation follows approximately the same physical law for different flight condition. In the range of 65°—85° LOS angle, the imaging deviation first decreases and then increases, and the direction reverses. The magnitude of the imaging deviation is proportional to the angle of deflection and the direction follows the direction of the deflection angle.

The deflection angle $\delta$ between the boundary of the aero-optic flow field and the shock wave, and the deflection angle $\zeta$ from the shock wave to the optical window, always show opposite deflection direction at the same LOS angle, which means that there are two refraction laws for light in the aero-optic flow field, close to the normal and far from the normal.

During the propagation of light from the boundary of the aero-optical flow field to the optical window, the density distribution law is first rapidly increasing and then slowly decreasing. After the light enters the shock wave, it is rapidly refracted, and after passing through the shock wave, the refracted light starts to be revised slowly, and the angle of deflection gradually decreases. When the correction process is too extensive, the light is deflected in the opposite direction.

In the aero-optic flow field with the shock wave as the dividing line, the light propagation in the flow field is divided into two parts, the upper part is refracted close to the normal, the deflection angle is large but the propagation distance is too short; the lower part is deflected away from the normal, and the propagation distance is longer, which eventually causes the light from the flow field boundary to the optical window as the process of refraction away from the normal.

As suggested in the previous paper, the operating conditions in this paper belong to high altitude and high Mach number, and it is necessary to make more comprehensive analysis of the light propagation characteristics of different operating conditions in the future, and then explore the influence of related factors on practical applications. By combining the genetic algorithm to predict the imaging deviation, the results of this paper are expected to provide theoretical calculation reference for the design of flight altitude, velocity, angle of attack and imaging attitude of infrared guided vehicles.

## Ethics declarations

## Conflicts of interest

The authors declare no conflict of interest.

## References

[1] FRUMKER E, PADE O. Generic method for aero-optic evaluations[J]. Applied optics, 2004, 43(16): 3224-3228.

[2] DING H, YI S, XU Y, et al. Recent developments in the aero-optic effects of high-speed optical apertures: from transonic to high-supersonic flows[J]. Progress in aerospace sciences, 2021, 127: 100763.

[3] BIAN Z, LI J, GUO L. Simulation and feature extraction of the dynamic electromagnetic scattering of a hypersonic vehicle covered with plasma sheath[J]. Remote sensing, 2020, 12(17): 2740.

[4] WANG H, CHEN S, DU H J, et al. Influence of altitude on aero-optic imaging quality degradation of the hemispherical optical dome[J]. Applied optics, 2019, 58(2): 274-282.

[5] PALHARINI R C, SCANLON T J, WHITE C. Chemically reacting hypersonic flows over 3D cavities: flowfield structure characterisation[J]. Computers & fluids, 2018, 165: 173-187.

[6] GUO G, LUO Q. DSMC investigation on flow characteristics of rarefied hypersonic flow over a cavity with different geometric shapes[J]. International journal of mechanical sciences, 2018, 148: 496-509.

[7] GUAN Y, SANG X, XING S, et al. Backward ray tracing based high-speed visual simulation for light field display and experimental verification[J]. Optics express, 2019, 27(20): 29309-29318.

[8] WANG H, CHEN S, DU H J, et al. Influence of altitude on aero-optic imaging quality degradation of the hemispherical optical dome[J]. Applied optics, 2019, 58(2): 274-282.

[9] GUO G, LIU H, ZHANG B. Aero-optical effects of an optical seeker with a supersonic jet for hypersonic vehicles in near space[J]. Applied optics, 2016, 55(17): 4741-4751.

[10] YAO Y, XUE W, WANG T, et al. Influence of LOS angle on aero-optics imaging deviation[J]. Optik, 2020, 202: 163732.

[11] WANG L, XU L, ZHAO S, et al. Influence of 0°–15° attack angle on aero-optical imaging deviation of a blunt-nose vehicle[J]. Applied optics, 2023, 62(2): 391-397.

[12] XU L, CAI Y. Imaging deviation through non-uniform flow fields around high-speed flying vehicles[J]. Optik, 2012, 123(13): 1177-1182.

[13] XU L, CAI Y. Influence of altitude on aero-optic imaging deviation[J]. Applied optics, 2011, 50(18): 2949-2957.

[14] SAXTON-FOX T, MCKEON B J, GORDEYEV S. Effect of coherent structures on aero-optic distortion in a turbulent boundary layer[J]. AIAA journal, 2019, 57(7): 2828-2839.

[15] SAHBA S, SASHIDHAR D, WILCOX C C, et al. Dynamic mode decomposition for aero-optic wavefront characterization[J]. Optical engineering, 2022, 61(1): 013105-013105.

[16] OH K, CHOI K, LEE S, et al. Aerodynamic and aero-

optic computation of a lateral jet-controlled high-speed vehicle operating at medium altitudes[C]//APISAT 2019: Asia Pacific International Symposium on Aerospace Technology, December, 2019, Gold Coast, Australia. CSAA, RAeS Australian Division, KSAS, JSASS, 2019: 899-911.

[17] HAO C, CHEN S, ZHANG W, et al. Comprehensive analysis of imaging quality degradation of an airborne optical system for aerodynamic flow field around the optical window[J]. Applied optics, 2013, 52(33): 7889-7898.

[18] KETIAN S H I, HANDONG M A. Progress in computational aero-optics[J]. Acta aerodynamica sinica, 2019, 37(2): 186-192.

[19] YAMAZAKI K. Nonuniqueness in law for two-dimensional Navier-Stokes equations with diffusion weaker than a full Laplacian[J]. SIAM journal on mathematical analysis, 2022, 54(4): 3997-4042.

[20] YIN K, JIANG H. Evaluations on aero-optic effects of subsonic airborne electro-optical system[J]. Chinese optics letters, 2006, 4(8): 435-438.

[21] ZHAO X, YI S, DING H. Experimental study on the influence of attitude angle on the aero-optic effects of a hypersonic optical dome[J]. Optik, 2020, 201: 163448.

[22] GAUDET B, FURFARO R, LINARES R. Reinforcement learning for angle-only intercept guidance of maneuvering targets[J]. Aerospace science and technology, 2020, 99: 105746.

[23] XU L, ZHANG Z, WANG T, et al. Numerical study on aero-optic imaging deviations of vehicles at different altitudes[J]. Optoelectronics letters, 2022, 18(2): 97-102.

[24] LEE S, LEE B J, JEUNG I S. Wavefront distortion due to the shock wave and boundary layer in the supersonic flow over a compression ramp[J]. Aerospace science and technology, 2021, 110: 106489.

[25] CAO L, ZHANG B, HOSSAIN M D M, et al. Tomographic reconstruction of light field PIV based on a backward ray-tracing technique[J]. Measurement science and technology, 2021, 32(4): 044007.